ACS EARTH AND SPACE CHEMISTRY

http://pubs.acs.org/journal/aesccq

Article

Simulation of Monoterpene SOA Formation by Multiphase Reactions Using Explicit Mechanisms

Zechen Yu, Myoseon Jang,* Tianyu Zhang, Azad Madhu, and Sanghee Han

Cite This: *ACS Earth Space Chem.* 2021, 5, 1455−1467

Read Online

ACCESS | Metrics & More | Article Recommendations | Supporting Information

ABSTRACT: The formation of terpene secondary organic aerosol (SOA) was simulated using the unified partitioning aerosol phase reaction model that predicted multiphase reactions of hydrocarbons in the presence of electrolytic inorganic aerosols. To predict oxygenated products from the atmospheric oxidation of terpenes, the master chemistry mechanism, an explicit gas kinetic mechanism, was implemented. The resulting products were then classified into 51 lumping groups using mass-based stoichiometric coefficients according to their volatility and aerosol phase reactivity. In the presence of wet inorganic aerosol, the SOA model was approached by liquid−liquid phase separation between the organic and inorganic phases due to the hydrophobicity of terpene products (oxygen to carbon ratios <0.6). The model streamlined three SOA formation pathways including partitioning of gaseous oxidized products onto both the organic aerosol and aqueous aerosol phases, oligomerization in the organic phase, and aqueous phase reactions (acid-catalyzed oligomerization and organosulfate formation). In the model, the peroxy radical autoxidation mechanism, which is a recently derived explicit mechanism to form highly oxygenated molecules, was also included to form less volatile products. The model simulation was demonstrated for SOA data that were produced through the photo-oxidation of three different monoterpenes (α-pinene, β-pinene, and D-limonene) under various experimental conditions in a large outdoor photochemical smog chamber. Terpene SOA growth was considerably accelerated in the aqueous phase anchored in acidic seeds but much weaker with neutral seeds. This tendency is quite different from that of isoprene SOA, which noticeably grows even in the neutral aqueous phase. Unlike hydrophilic isoprene products, terpene products are hydrophobic and weakly soluble in the aqueous phase, and thus, the neutral aqueous phase is insufficient to increase SOA mass. The model underestimated the production of polar functional groups, such as −OH, −COOH, and $-ONO_2$, compared to the compositions measured using Fourier-transform infrared spectral data. In particular, the model underestimated carboxylic acids due to the knowledge gaps in the mechanisms to form carboxylic acid in both gas-phase oxidation and in-particle chemistry. Under the current emission trends in which SO_2 and NO_x have been decreasing, the model simulation suggested that the reduction of sulfate is more efficient to reduce SOA mass than the reduction of NO_x.

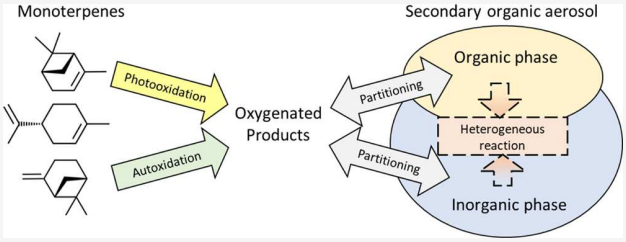

KEYWORDS: *secondary organic aerosol, SOA model, monoterpene SOA, photooxidation, autoxidation*

1. INTRODUCTION

Secondary organic aerosol (SOA) represents a significant proportion of ambient tropospheric aerosol and influences climate forcing[1,2] and human health.[3] Monoterpenes, biogenic hydrocarbons, yield a significant amount of SOA with an annual global SOA production rate of 19.9 Tg y^{-1}, which is 50.3% of the total biogenic SOA.[4] In remote areas, approximately half of the summertime SOA is reported from monoterpene oxidation.[5] In addition, terpene SOA formation rapidly progresses because of the fast reactivity of terpene with atmospheric oxidants (i.e., OH radicals, ozone, and nitrate radicals).[1,6] The products from terpene oxidation may self-nucleate, partition onto pre-existing particulate matter, or undergo aerosol phase reactions to form SOA.[7−11] The SOA yields of monoterpenes varied with precursor hydrocarbons and NO_x levels.[12−14] Hence, monoterpenes can also significantly contribute to the global SOA budget due to their nature of producing high yields of low-volatility products during the atmospheric process.[15,16]

Predictive SOA models have been developed over time to provide feasible tools for understanding SOA impact on climate and human health. The early gas−particle partitioning model utilizes a classical partitioning theory as the backbone for SOA growth.[17] By using simple model parameters for two[18] or more surrogate products,[19] these partitioning-based SOA models semiempirically established a relationship between the absorbing organic mass (OM) concentration and SOA yields.

Received: February 28, 2021
Revised: April 14, 2021
Accepted: April 30, 2021
Published: May 12, 2021

This gas−particle partitioning mode has been widely implemented in regional and global models due to its simplicity and efficiency in calculation. However, the predictability of the partitioning-based SOA model is limited due to the missing SOA formation pathway when the electrolytic inorganic aerosol is present. Over the last two decades, numerous studies have shown that aerosol-phase reactions of some organic species (i.e., aldehydes and epoxides)[20−22] can yield nonvolatile oligomers, resulting in increases in SOA mass. Furthermore, aerosol-phase reactions to form oligomers can be increased in the presence of an aqueous phase and accelerated by an acid catalyst[1,8] associated with acidic inorganic aerosol. In order to consider emerging chemistry, the SOA model needs to link the physicochemical properties of organic products to both atmospheric conditions (humidity, temperature, and NO_x levels) and aerosol environments [acidity, aerosol liquid water content (LWC), and inorganic compositions] in the presence of electrolytic inorganic aerosol. For example, the gas−aerosol model for mechanism analysis was developed by McNeill et al. to predict the formation of isoprene SOAs via aqueous-phase chemistry.[23] Dawson et al.[24] developed a gas-phase and SOA model (aroCACM/MPMPO) including oxidation of aromatics by assuming the condensed phase as a simple mixed inorganic phase or organic−inorganic separate phase. Couvidat and Sartelet Couvidat and Sartelet[25] designed the SOA processor (SOAP v1.0) by implementing morphology factors accounting for aerosol physical heterogeneity and organic diffusions. Jang et al. recently launched the unified partitioning aerosol phase reaction (UNIPAR) model, including the partitioning process and aerosol phase reactions of oxygenated products originating from gas mechanisms of hydrocarbons (HCs).[9,26−28] The UNIPAR model has recently been evaluated by Im and Jang,[27] and Zhou[28] for aromatic HCs such as toluene, ethylbenzene, propylbeneze, and 1,3,5-trimethylbenzene with an assumption of liquid−liquid phase separation (LLSP) between the inorganic phase and organic phase. Beardsley and Jang extended UNIPAR to the prediction of isoprene SOA assuming a single homogeneously mixed phase (SHMP) between inorganic and organic phases.[26]

In addition to aerosol-phase reactions, several recent studies suggested that atmospheric autoxidation of monoterpene in the gas phase can be one of the missing chemical pathways.[16,29,30] The formation of highly oxygenated molecules (HOMs), which are formed through the autoxidation of peroxy radicals, has also been experimentally identified.[31−36] For monoterpenes, HOM formation starts with ozonolysis,[14] followed by the addition of O_2 to form peroxyl radicals. Furthermore, peroxyl radicals can form epoxide and alkoxyl radicals of monoterpenes via the intramolecular rearrangement of H atoms [abstraction of allylic H atoms (H-shift) or addition of H to the unsaturated C═C bond]. Multigeneration autoxidation increases ketone and hydroxyl functional groups in products.[16,31] The peroxy radical autoxidation mechanism (PRAM) has been recently developed by Roldin et al. based on experimental observations and the theoretical study of monoterpene oxidation.[37,38] Despite the relatively low yield of HOMs, their low volatility with a high O/C (>0.7) is capable of driving initial nanoparticle growth and substantially impacting the total SOA mass.[30]

In this study, the SOA formation via multiphase reactions of three terpenes (α-pinene, β-pinene, and D-limonene) was simulated using the UNIPAR model. The oxygenated products originating from the explicit gas mechanisms [master chemistry mechanisms (MCMs), version v3.3.1][39] were applied to partitioning and in-particle chemistry. In the presence of wet inorganic aerosol, the aerosol phase is considered as LLPS because terpene products were relatively hydrophobic (oxygen to carbon ratios: 0.3−0.6).[40−43] Additionally, the impact of HOMs on SOA formation was demonstrated by adding the recently reported autoxidation mechanisms by Roldin et al.[37] The simulated SOA mass was examined against the chamber-generated SOA data that were produced from the photo-oxidation of three different monoterpenes (α-pinene, β-pinene, or D-limonene) under varying NO_x levels (HC/NO_x > 5.5 and <5.5 ppbC/ppb) and seed conditions [i.e., no seed (NS), wet ammonium sulfate (wAS), and sulfuric acid (SA)]. The simulated SOA compositions were also compared with the functional group compositions that were constructed by using Fourier-transform infrared (FTIR) spectral data. The sensitivity of the three terpene SOAs to environmental variables, such as temperature, relative humidity (RH), aerosol acidity, and NO_x levels, was thoroughly demonstrated using the model.

2. METHODOLOGY

2.1. Outdoor Chamber Experiments. Terpene SOA was produced from photo-oxidation of three different HCs (α-pinene, β-pinene and D-limonene) using the Atmospheric PHotochemical Outdoor Reactor (UF-APHOR) dual chamber (52 m^3 each) located at the University of Florida. A detailed description of the operation of the large outdoor smog chamber has been described previously.[26,28,44−46] In summary, HCs were evaporated into the outdoor chamber with heating. 400 ppb of non-reactive CCl_4 (Sigma-Aldrich; ≥99.5%) was used as the indicator for chamber dilution. HCs and NO (2% in N_2, Airgas Inc., USA) were introduced into the smog chamber before sunrise. For each HC, two different NO_x levels (high NO_x: HC/NO_x < 5 ppbC/ppb; low NO_x: HC/NO_x > 10 ppbC/ppb) and three different seed conditions (without seed; SA; and ammonium sulfate, AS) were studied. The concentration of gas-phase HCs was monitored by GC-FID (7820A, Agilent Technologies, Inc., USA). The concentrations of ozone and NO_x were measured using a photometric ozone analyzer (400E, Teledyne Technologies, Inc., USA) and a chemiluminescence NO/NO_x analyzer (T201, Teledyne Technologies, Inc., USA), respectively.

For the experiments in the presence of the inorganic seed, the inorganic ion concentration was monitored using a particle into liquid sampler (ADISO 2081, Applikon Inc., USA) integrated with ion chromatography (Compact IC 761, Metrohm Inc., Switzerland) (PILS-IC). The particle size distribution was monitored using a scanning mobility particle sizer (SMPS 3080, TSI Inc., USA). The meteorological factors, such as temperature, relative humidity (RH), and sunlight intensity, were monitored both inside and outside the smog chamber using a hygrometer (CR1000 measurement and control system, Campbell Scientific Inc., USA) and an ultraviolet radiometer (TUVR, Eppley Laboratory Inc., USA), respectively. SOA mass was simulated by using the meteorological variables that were measured during the chamber experiment. To study the effect of aerosol LWC on SOA formation, the experiments in the presence of inorganic seeds were performed under controlled RH conditions. For dAS-seeded experiments, RH was controlled less than the efflorescence RH (ERH) of the AS seed, and for wAS-seeded experiments, RH was maintained higher than 50% to prevent

https://doi.org/10.1021/acsearthspacechem.1c00056
ACS Earth Space Chem. 2021, 5, 1455−1467

seed crystallization. The time profiles of RH and temperature for the dry and wet experiments are shown in Figure S1. The concentration of organic carbon in aerosol was monitored using an organic carbon/elemental carbon aerosol analyzer (OC/EC model 4, Sunset Laboratory Inc., USA) every 50 min. The concentration of organic matter in aerosol (OM, $\mu g\ m^{-3}$) was then calculated based on the measured OC concentration and an OM to OC ratio. The averaged OM to OC ratio of all three terpene SOAs is set to 1.7 based on the measurement using OC/EC and filter mass. The concentration of OM produced in the chamber was corrected for both chamber dilution using the dilution factor and the particle loss to the chamber wall using a particle-loss factor. The measured maximum OM mass concentration ranged from 8.3 to 83.4 $\mu g\ m^{-3}$ in this study. The aerosol composition (sulfate, nitrate, ammonium, and OM) was also monitored using an aerosol chemical speciation monitor (ACSM, Aerodyne Research Inc., USA). The resulting ACSM compositions were compared with the data obtained from OC and PILS-IC. SOA yields (Y) were then calculated as the maximum concentration of OM divided by the consumption of HC precursors. According to the previous studies by Aiken, et al.[47] and Canagaratna, et al.,[48] the O/C ratio of SOA can be calculated using an empirical equation based on the measured f_{44} (ACSM data). As listed in Table S1, the estimated O/C ratio of the SOA collected in this study ranges from 0.3 to 0.58, which is similar to the reported literature values of 0.3−0.6.[41] The detailed experimental conditions of outdoor chamber experiments are summarized in Table S1. An example of the typical time profiles of concentrations of HCs, NO_x, and O_3 is shown in Figure S2 in the Supporting Information. An example of the time profiles of total ultraviolet radiation that was measured in the UF-APHOR chamber is shown in Figure S3.

2.2. Characterization of SOA Composition Using FTIR. The functional groups of aerosol samples were characterized using a FTIR spectrometer (Nicolet iS50, Thermo Fisher Inc., USA). The SOA was collected by impaction onto a silicon optical disc (13 × 2 mm, Sigma-Aldrich, USA) using a specially fabricated sampling holder. For the SOA produced at low NO_x levels (Table S1), the aerosol sampling began near noon when the SOA mass was at the maximum. The duration of the sample collection was 90 min. The aerosol mass collected on the FTIR disc was determined by measuring the mass difference before and after the aerosol collection using an analytical balance (MX5, Mettler-Toledo Ltd, Columbus, OH). The aerosol mass that was collected on the FTIR disc ranged from 20 to 50 μg. Immediately after sampling aerosols on the FTIR disc, aerosol functional groups were analyzed using the FTIR spectrometer. A DTGS detector was used for the analysis. The FTIR spectra were obtained in the absorbance mode ranging from 800 to 4000 cm^{-1} with a resolution of 0.121 cm^{-1} and a scan number of 8. The software Omnic version 9 (Thermo fisher scientific Inc.) was used for the collection of FTIR spectra and post-process. The detailed experimental conditions for the SOA used in FTIR studies are shown in Table S1. The functional group compositions (C−H, O−H, C═O, C(═O)O−H, and nitrate) of each SOA were constructed using the decoupled FTIR spectra.[21,49]

2.3. Determination of Aerosol Acidity. In this study, the aerosol proton concentration ($[H^+]$, mol L^{-1} of aerosol) was measured using colorimetry integrated with a reflectance UV−visible spectrometer (C-RUV).[50] For SA-seeded experiments, the aerosol acidity can be reduced by either the neutralization of SA with ammonia gas or the formation of dialkyl organosulfates (diOSs). The acidity of the aqueous aerosol phase is an important parameter to accelerate the in-particle chemistry of organic products.[8] The change in $[H^+]$ associated with ammonia neutralization can be determined using the conventional inorganic thermodynamic model (i.e., EAIM-II)[51,52] based on the inorganic composition obtained from PILS-IC measurements. The C-RUV method detects the $[H^+]$ originating from both the ammonia neutralization and diOS formation. The quantity of diOS is determined by using the difference between the traditional $[H^+]$ estimation using the inorganic thermodynamic model and the $[H^+]$ determined using C-RUV.[53]

3. DESCRIPTION OF THE UNIPAR MODEL

The UNIPAR model was previously evaluated for aromatic SOA in the presence of electrolytic inorganic aerosol[28] in the LLPS mode and also demonstrated for isoprene SOA in the SHMP mode.[26] In this study, the UNIPAR model was extended to the prediction of SOA formation via multiphase oxidation of monoterpene. The overall structure of the UNIPAR model is illustrated in Figure 1. For terpene SOA,

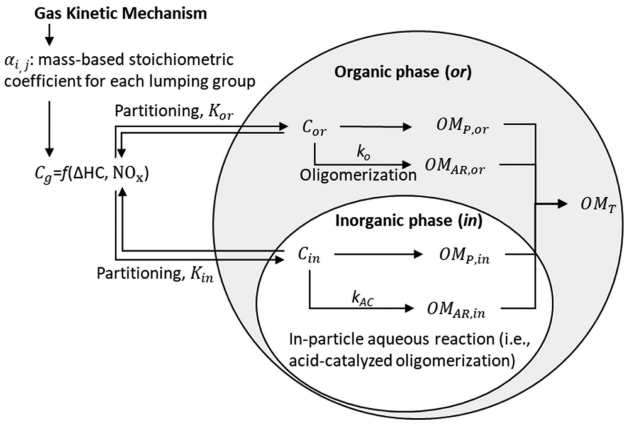

Figure 1. Scheme of the UNIPAR model. $\alpha_{i,j}$ (i: reactivity level; and j: vapor pressure level) is the mass-based stoichiometric coefficient of the lumping group simulated from the gas kinetic mechanisms (MCM v3.3.1 and PRAM). C_g, C_{or}, and C_{in} represent the concentration of the lumping species in the gas phase (g), organic phase (or), and inorganic phase (in), respectively. K_{or} and K_{in} are the partitioning coefficient of lumping species from the gas phase to the organic phase and from the gas phase to the inorganic phase, respectively. k_o and k_{AC} are the reaction rate constant of the in-particle reaction in the organic phase and inorganic phase, respectively. OM_p, OM_{AR}, and OM_T are the OM formed from the partitioning process, aerosol-phase reactions, and total OM, respectively.

simulations were performed in the LLPS mode due to the relatively large hydrophobicity of SOA products showing low O/C ratios (<0.6).[40−42] In the model, the total OM (OM_T, $\mu g\ m^{-3}$) is attributed to the OM (OM_p, $\mu g\ m^{-3}$) formed through multiphase partitioning and the OM (OM_{AR}, $\mu g\ m^{-3}$) originating from in-particle chemistry (i.e., oligomerization in the organic phase, acid-catalyzed reactions in the aqueous phase, and diOS formation).

3.1. Gas-Phase Mechanisms and Lumping of Gas Products. The oxidation of the terpene in the gas phase was simulated using the explicit gas-phase chemistry mechanism (MCM, v3.3.1)[39,54,55] on the box model platform using the

https://doi.org/10.1021/acsearthspacechem.1c00056
ACS Earth Space Chem. 2021, 5, 1455−1467

Dynamically Simple Model for Atmospheric Chemical Complexity (DSMACC).[46,56] In order to simulate HOMs via the gas-phase autoxidation of terpene products, the PRAM[57] was added to the MCM. The standard NO_x-dependent distributions of gas-phase products were simulated by varying NO_x levels (HC/NO_x = 2−50 ppbC/ppb) under given meteorological conditions (sunlight intensity, temperature, and RH on June 19, 2015). The resulting products were lumped into 51 groups within a two-dimensional array: eight levels of volatility (10^{-8}, 10^{-6}, 10^{-5}, 10^{-4}, 10^{-3}, 10^{-2}, 10^{-1}, and 1 mm Hg) and six levels of aerosol-phase reactivity [very fast (VF); fast (F); medium (M); slow (S); partitioning only (P); and multi-alcohol (MA)] plus three additional reactive species (glyoxal: GLY; methylglyoxal: MGLY; and epoxydiols: IEPOX) with their own vapor pressure. The aerosol-phase reactivity represents the reactivity of the organic species in aerosol-phase reactions (i.e., oligomerization). A detailed description of the lumping criteria and the mass-based stoichiometric coefficient (α_i) of the lumping group i can be found in previous studies.[28] In the previous study by Zhou et al.,[28] α_i was reconstructed to simulate the atmospheric aging of monoalkylbenzene SOA (toluene, ethylbenzene, and propylbenzene). Terpenes are highly reactive and quickly oxidized to form SOA. Unlike monoalkylbenzene, terpenes rapidly oxidize at low NO_x levels and their α_i of the oxidation products is less sensitive to the atmospheric aging over the day of the experiment under ambient sunlight. The α_i at high NO_x levels changes with atmospheric aging, which is a function of radical concentrations (relative concentration of HO_2 and RO_2 normalized by the initial HC concentration). After simulation of the oxidation of each terpene in the gas phase, the oxygenated products are classified into 51 lumping species as shown in Tables S2−S8.

3.2. GasAerosol Partitioning. For the OM_P estimation, the lumped species produced in the gas (g) phase are distributed into both the inorganic (in) phase and organic (or) phase by gas-aerosol absorptive partitioning theory.[17] The partitioning coefficients of each product i between the gas and organic phase ($K_{or,i}$, m^3 μg^{-1}) and between the gas and inorganic phase ($K_{in,i}$, m^3 μg^{-1}) are estimated as follows

$$K_{or,i} = \frac{7.501RT}{10^9\ MW_{or}\gamma_{or,i}p^{o}_{l,i}} \tag{1}$$

$$K_{in,i} = \frac{7.501RT}{10^9\ MW_{in}\gamma_{in,i}p^{o}_{l,i}} \tag{2}$$

where R (8.314 J mol^{-1} K^{-1}) is the ideal gas constant and T (K) represents temperature. MW_{or} (g mol^{-1}) and MW_{in} (g mol^{-1}) represent the averaged molecular weight of organic media and inorganic media, respectively. $p^{o}_{l,i}$ (mmHg) represents the subcooled liquid vapor pressure of the product i and is estimated using the group contribution method.[58−60] The activity coefficient of i in the or phase ($\gamma_{or,i}$) is assumed to be unity.[61] The activity coefficient of i in the in phase ($\gamma_{in,i}$) was semiempirically calculated by regression of the model-predicted activity coefficients of various organic products using a thermodynamic model (AIOMFAC)[62] to aerosol parameters [i.e., RH and fractional sulfate (FS = $[SO_4^{2-}]/([SO_4^{2-}]+[NH_4^+])$] and physicochemical parameters of i [i.e., the molecular weight (MW_i, g mol^{-1}), oxygen to carbon ratio (O/C_i), and hydrogen bonding (HB_i) parameter].

$$\gamma_{in,i} = e^{0.035MW_i - 2.704\ln(O:C_i) - 1.121HB_i - 0.33FS - 0.022(100RH)} \tag{3}$$

The calculated activity coefficients of the organic products in the inorganic phase range from 10 to 10^7 within the simulations of this study. The partitioning model to predict SOA formation was originally developed by Schell et al.[63] and was reconstructed by Cao and Jang[64] to exclude nonvolatile OM formed through the aerosol-phase reaction ($OM_{AR,i}$, μg m^{-3}). OM_P is then estimated from the total concentration of species i ($C_{T,i}$, μg m^{-3}) using a mass balance equation as a function of the effective saturation concentration ($C^*_{g,i} = 1/K_{or,i}$).

$$OM_P = \sum_i \left[C_{T,i} - OM_{AR,i} - C^*_{g,i}\frac{\frac{C_{or,i}}{MW_i}}{\sum_i\left(\frac{C_{or,i}}{MW_i} + \frac{OM_{AR,i}}{MW_{oli,i}}\right) + OM_0} \right] \tag{4}$$

where OM_0 (mol m^{-3}) is the concentration of the pre-existing OM, $MW_{oli,i}$ (g mol^{-1}) is the molecular weight of the dimer, and $C_{or,i}$ (μg m^{-3}) is the concentration of species i in the organic phase. As $C_{or,i}$ is unknown in the absorbing medium ($\sum_i\left(\frac{C_{or,i}}{MW_i} + \frac{OM_{AR,i}}{MW_{oli,i}}\right) + OM_0$, in eq 4), OM_P was solved by the iteration method using a globally convergent Newton−Raphson method.[65]

3.3. In-Particle Chemistry. $OM_{AR,i}$ is calculated as a sum of the OM formed by both oligomerization in the organic phase ($OM_{AR,or,i}$, μg m^{-3}) and oligomerization in the inorganic phase ($OM_{AR,in,i}$, μg m^{-3}). $OM_{AR,in,i}$ is assumed to be processed through the self-dimerization reaction (second-order reaction).[66] In the presence of an acid catalyst, the oligomerization can be accelerated.[8] The kinetic equations of the oligomerizations in the organic phase and inorganic phase are shown as follows

$$\frac{dC_{or,i}}{dt} = -k_{o,i}C'^{2}_{or,i}\left(\frac{MW_iOM_T}{\rho_{or}10^3}\right) \tag{5}$$

$$\frac{dC_{in,i}}{dt} = -k_{AC,i}C'^{2}_{in,i}\left(\frac{MW_iM_{in}}{\rho_{in}10^3}\right) \tag{6}$$

where $k_{o,i}$ (L mol^{-1} s^{-1}) and $k_{AC,i}$ (L mol^{-1} s^{-1}) are the oligomerization rate constant in the organic phase and inorganic phase, respectively. ρ_{in} is the density of the inorganic aerosol and calculated from the regression equation through the E-AIM model. ρ_{or} (1.38 g mL^{-1}) is the averaged density of terpene organic aerosols.[67−69] According to the method developed by Jang et al.,[70] $k_{AC,i}$ and $k_{o,i}$ can be semiempirically estimated as a function of species reactivity (R_i), protonation equilibrium constant (pK_{BH^+i}), excess acidity (X), water activity (a_w), and proton concentration ($[H^+]$).

$$k_{AC,i} = 10^{0.846R_i + 0.22pK_{BH^+i} + 1.003\cdot X + \log(a_w[H^+]) - 2.8} \tag{7}$$

$$k_{o,i} = 10^{0.846R_i + 0.22pK_{BH^+i} - 4.9} \tag{8}$$

https://doi.org/10.1021/acsearthspacechem.1c00056
ACS Earth Space Chem. 2021, 5, 1455−1467

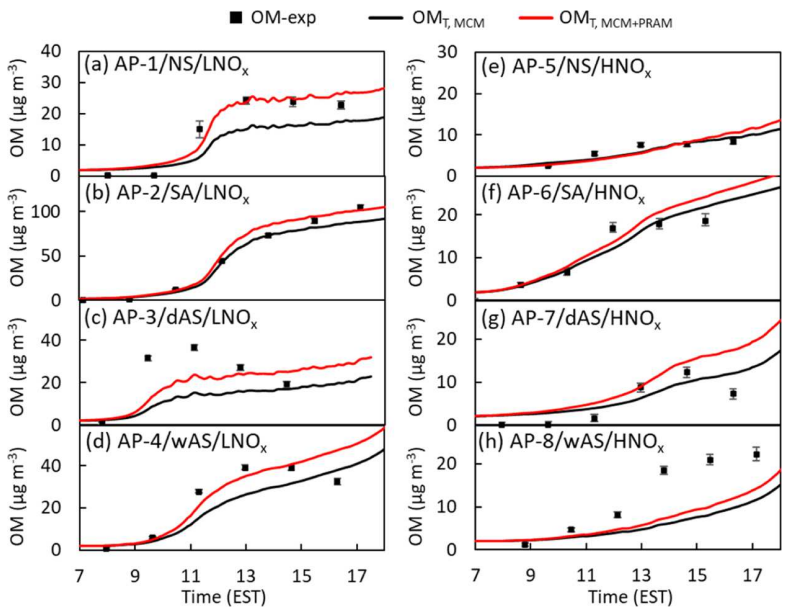

Figure 2. Time profiles of measured OM (OM-exp) vs simulated OM formed from photo-oxidation of α-pinene (AP) at low NO_x (LNO_x: HC/NO_x > 10 ppbC/ppb) levels with the seed conditions of (a) NS, (b) SA, (c) dAS, and (d) wAS and at high NOx (HNO_x: HC/NO_x < 5 ppbC/ppb) levels with the seed conditions of (e) NS, (f) SA, (g) dAS, and (h) wAS. OM_T represents total OM concentration. "MCM" and "MCM + PRAM" denote the simulations performed with MCM v3.3.1 only and with the additional proxy radical autoxidation mechanism (PRAM), respectively.

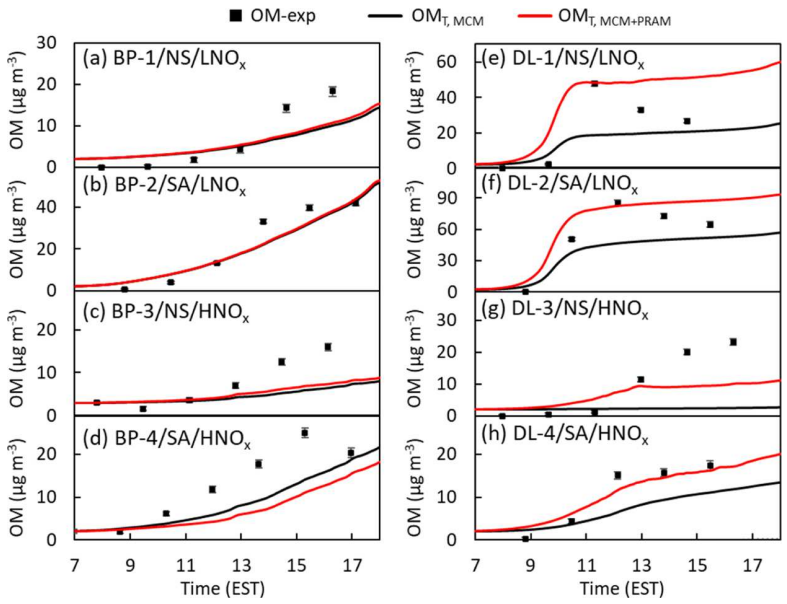

Figure 3. Time profiles of simulated OM vs. experimentally observed OM (OM-exp) for β-pinene SOA (BP) at(a) LNO_x (HC/NO_x > 10 ppbC/ppb) without seed (NS), (b) LNO_x with SA seed, (c) HNO_x (HC/NO_x < 5 ppbC/ppb) without seed, and (d) HNO_x with SA and for D-limonene SOA (DL) at (e) LNO_x without seed, (f) LNO_x with SA, (g) HNO_x without seed, and (h) HNO_x with SA. OM_T represents the total OM concentration. "MCM" and "MCM + PRAM" denote the simulations performed with the MCM v3.3.1 only and with the MCM integrated with the PRAM.

The acidic sulfate in aerosols can be neutralized by ammonium or converted to diOS via esterification. This further affects aerosol acidity and hygroscopicity. Using a previously developed equation,[50] diOS concentration ($[diOS]_{model}$, $\mu g\ m^{-3}$) is predicted as a function of free sulfate ($[SO_4^{2-}]_{free}$, $\mu g\ m^{-3}$), which is available for neutralization and organic physicochemical properties which are related to effectiveness to form diOS (Supporting Information Section S3). For SOA simulation, the concentrations of ammonium ions from the PILS-IC data were also used for the calculation of aerosol acidity and diOS formation.

4. RESULTS AND DISCUSSION

4.1. Simulated SOA Formation. The SOA formation from three terpenes, α-pinene, β-pinene, or D-limonene, was simulated using the UNIPAR model under the measured

https://doi.org/10.1021/acsearthspacechem.1c00056
ACS Earth Space Chem. 2021, 5, 1455−1467

SOA system	SOA yield (%) at different model variables							
	Temperature =298 K				Temperature = 278 K			
	RH = 45%		RH = 80%		RH = 45%		RH = 80%	
	High NO_x	Low NO_x	High NO_x	Low NO_x	High NO_x	Low NO_x	High NO_x	Low NO_x
AP/NS	1.6%	6.1%	1.6%	6.1%	6.2%	19.1%	6.2%	19.1%
AP/AS	1.9%	6.7%	2.2%	7.4%	7.0%	20.0%	7.6%	20.0%
AP/AHS	4.8%	10.0%	5.6%	11.3%	11.1%	24.9%	12.0%	26.6%
BP/NS	0.6%	1.6%	0.6%	1.6%	2.3%	4.7%	2.3%	4.7%
BP/AS	0.8%	2.6%	0.9%	2.9%	3.1%	6.5%	3.7%	7.1%
BP/AHS	2.1%	4.6%	2.4%	5.0%	4.4%	8.9%	5.0%	9.7%
DL/NS	1.5%	10.8%	1.5%	10.8%	3.4%	18.4%	3.4%	18.4%
DL/AS	1.7%	11.2%	1.7%	11.3%	4.0%	18.9%	4.4%	19.2%
DL/AHS	2.8%	13.8%	3.2%	14.5%	6.5%	20.9%	6.9%	21.3%

Figure 4. Sensitivity of the predicted SOA yield to the model parameters. "High NO_x" and "Low NO_x" represent the high NO_x level (HC/NO_x = 3 ppbC/ppb) and low NO_x level (HC/NO_x = 15 ppbC/ppb), respectively. "AP", "BP", and "DL" denote α-pinene, β-pinene, and D-limonene, respectively. "NS", "AS", and "AHS" represent the simulation in the absence of the seed, in the presence of the $(NH_4)_2SO_4$ seed, and in the presence of the NH_4HSO_4 seed, respectively. All simulations were performed with the initial concentration of 30 ppb HC precursor using the UNIPAR and MCM (v3.3.1) integrated with the PRAM under the reference sunlight profiles (June 19, 2015) from 6:30 to 17:30 (Figure S2). For simulations, 20 μg m^{-3} sulfate in the presence of AS and AHS and 2 μg m^{-3} preexisting OM_0 were included. The blue bar indicates the relative scale comparison between simulations.

meteorological conditions and compared with the experimental data obtained from the UF-APHOR chamber. Figure 2 shows the measured and the predicted α-pinene SOA formation in the presence of four different seeds including NS, SA, dAS, and wAS at two NO_x levels: high NO_x level (HC/NO_x < 5 ppbC/ppb) and low NO_x level (HC/NO_x > 10 ppbC/ppb). The simulated OM_p and OM_{AR} for three terpenes are shown in Figures S5 and S6.

Overall, SOA formation of α-pinene was reasonably predicted except that at high NO_x levels in the presence of wet AS (Figure 2h). Compared to the SOA yields in the absence of seeds (Figure 2a,e), the SOA yields in the presence of SA significantly increased due to the acid-catalyzed reactions (increased k_{AC}.)[26,71] in the aqueous inorganic phase (increased LWC). In the presence of acidic seeds, diOS forms through the esterification of sulfuric acid with reactive organic species (i.e., alcohols, aldehydes, and epoxides) and further influences aerosol acidity and hygroscopicity. The UNIPAR model captures the formation of diOS and dynamically modulates aerosol acidity associated with both the neutralization of sulfuric acid with gaseous ammonia and diOS formation. As shown in Figure S4, the observed diOS concentration using the C-RUV technique is well simulated by the model. The rapid change in $[H^+]$ in the morning originates from the decrease in LWC due to the reduction of RH. The diOS fraction in terpene SOA ranges from 3 to 10% under our experimental conditions, which is lower than the reported diOS formation in the SA-seeded aromatic SOA (6−15%)[28] and that in the SA-seeded isoprene SOA (~25%).[26] In the presence of wet AS (Figure 2d,h), SOA mass somewhat increased although less than that with acidic seed. No influence appeared on SOA yield with dAS compared to NS-SOA (Figure 2c,g). As shown in Figures 2e−h, the high NO_x level delayed SOA formation due to the suppression of the HO_x cycle via the reaction of NO_2 with OH radicals and consequently leads to the low SOA yield.

Figure 3 illustrates the SOA formation from the photooxidation of β-pinene or D-limonene in the absence and the presence of SA under two different NO_x levels. The promotion of SOA yields due to heterogeneous chemistry was also observed for both β-pinene and D-limonene SOA (Figure 3a,b,e,f). The rapid increase in SOA mass followed by a gradual SOA reduction appeared for the highly reactive terpenes (i.e., limonene) at low NO_x levels (Figure 2c,d,e,f) with a high concentration of terpene. At the beginning of the oxidation, the aerosol system temporarily becomes out of equilibrium because of the rapid terpene consumption and the production of a large number of new particles. A similar tendency was also found in other chamber studies for D-limonene SOA.[72]

Overall, SOA mass for β-pinene and D-limonene is underpredicted with the model: up to 50% in β-pinene (Figure 3c) and 57% in D-limonene (Figure 3g). Such an underestimation is plausibly due to missing mechanisms in both the gas-phase and in-particle chemistry. For example, Hammes et al.[73] reported the underestimation of the carboxylic acid formation for the simulation of the limonene oxidation by using MCM v3.3.1 (up to 56%).

To evaluate the impact of HOMs on SOA formation, the UNIPAR was also integrated with MCM-PRAM gas mechanisms.[37] In the presence of PRAMs, the predicted OM_T was increased because the PRAM-lumping species are less volatile (Table S8). Among the three terpenes in this study, D-limonene was most influenced by the PRAM because of its high path of the HOM precursor intermediate to the autoxidation mechanism. Evidently, the prediction of D-limonene SOA was improved with the MCM-PRAM as seen in Figure 3. Unlike HOM yields in α-pinene and D-limonene, those in β-pinene are trivial. Similar results were also observed in the previous studies.[16,74]

4.2. Sensitivities of SOA Prediction to Model Parameters. The sensitivities of SOA formation to temperature, RH, NO_x levels, and aerosol acidity were tested by simulating the UNIPAR model by changing each parameter under the reference sunlight (June 19, 2015 from 6:30 to 17:30 at UF-APHOR). The initial concentration of terpene was set to 30 ppb. Over the period of the simulation, the terpene was completely oxidized. For the impact of aerosol acidity and aerosol hygroscopicity on SOA, three different seeds were implemented: NS, wAS, and ammonium hydrogen sulfate (AHS). The results are shown in Figure 4 and the detailed

https://doi.org/10.1021/acsearthspacechem.1c00056
ACS Earth Space Chem. 2021, 5, 1455−1467

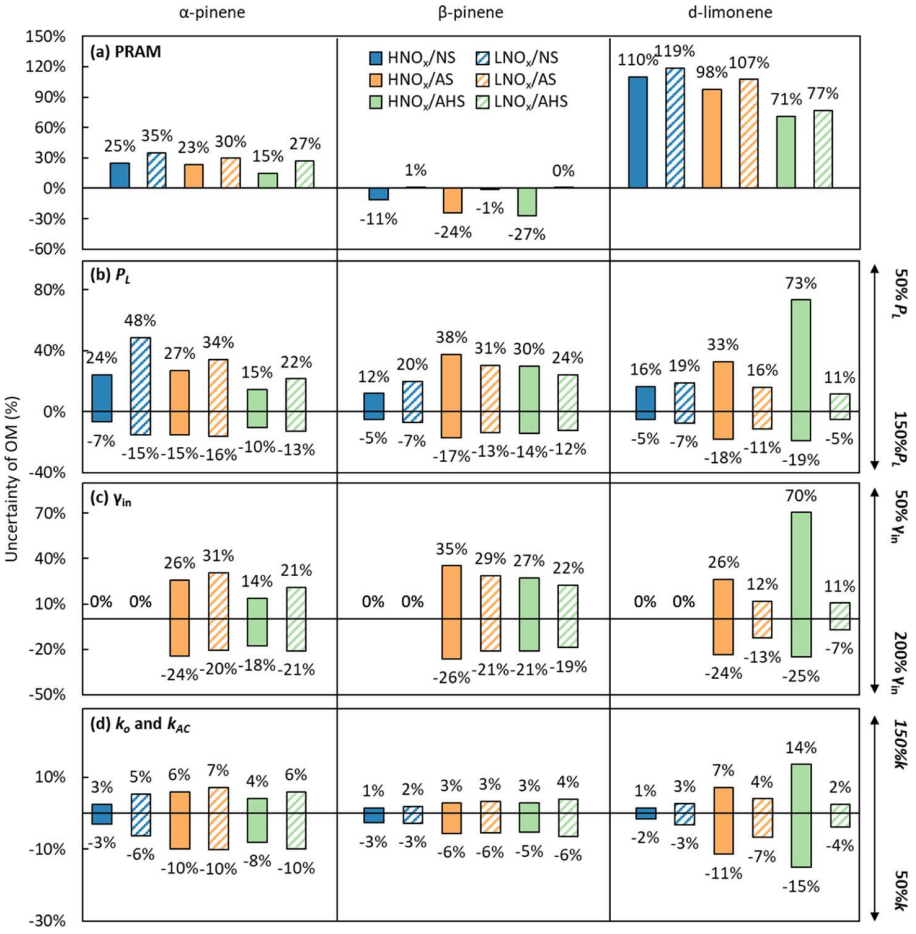

Figure 5. Uncertainties in the prediction of OM associated with (a) PRAMs, (b) vapor pressure (P_L), (c) activity coefficient (γ_{in}), and (d) reaction rate constant in the inorganic phase (k_{AC}) and in the organic phase (k_o). The errors associated with the PRAM were estimated with and without the PRAM. The errors associated with P_L, k_{AC}, and k_o were estimated by increasing and decreasing the factors by 150 and 50%. The uncertainties associated with γ_{in} were estimated through increasing and decreasing γ_{in} by 200 and 50%, respectively. For (b,c,d), OM_T was simulated using the UNIPAR and MCM (v3.3.1) integrated with the PRAM. All simulations were performed with an initial concentration of 30 ppb terpene at given reference meteorological profiles (June 19, 2015) from 6:30 to 17:30 (Figure S3). For simulations, 20 μg m^{-3} sulfate in the presence of AS and AHS and 2 μg m^{-3} preexisting OM_0 were included.

time profiles of SOA formation are shown in Figure S7−S9 (Supporting Information). The largest impacts on SOA yields appeared with temperature for all three terpenes. For example, SOA yields increased from 0.6−14.5% to 2.3−26.6% by decreasing temperature from 298 to 278 K. The increased organic concentration due to the reduction of vapor pressure at the lower temperature increases both OM_P and OM_{AR}. In the presence of wet inorganic seed, the impact of RH on SOA yields appeared to be small, although a high RH can increase the LWC of wet seeds. Unlike hydrophilic isoprene SOA products, terpene products are hydrophobic and weakly soluble in the aqueous phase. The low concentrations of products in the aqueous phase reduce the sensitivity of SOA yields to RH.

SOA yields of terpenes were significantly impacted by NO_x levels. By increasing the HC/NO_x ratio from 3 to 15 ppbC/ppb, the increased SOA yields for α-pinene, β-pinene, and D-limonene ranged from 200 to 370%, 190 to 330%, and 300 to 700%, respectively. The effect of NO_x levels on monoterpene SOA yield has been discussed by various studies.[75−77] At high NO_x levels, the reactions of NO_x with RO_2 lead to a more volatile product distribution and a lower SOA formation. Additionally, the autoxidation pathway from HOM precursor intermediates is suppressed at high NO_x levels. The effect of NO_x on SOA formation was the greatest in D-limonene due to the significant contribution of HOM to SOA mass.

As discussed in Section 3.3, the higher aerosol acidity promotes the higher SOA yields due to the acid-catalyzed heterogeneous reactions of organic compounds. D-Limonene is less sensitive to aerosol acidity compared to the other two terpenes, especially at the low NO_x levels. β-Pinene that has the least SOA yields was the most sensitive to acidity, as seen in Figure 4.

The partitioning mass (OM_P) fraction of the total SOA mass increases when the SOA simulation is equipped with autoxidation mechanisms as shown in Figure S10. The HOM fraction of total gas products also increases with decreasing hydrocarbon concentrations (Figure S10a). Some HOMs are less volatile, and they belong to groups 1S and 1P that dominantly partition to the aerosol phase in the UNIAPR model. Figure S10b shows the 1S+1P fraction to OM_P as the hydrocarbon concentration increases. We conclude that the OM_P fraction of the total SOA mass would be more important

https://doi.org/10.1021/acsearthspacechem.1c00056
ACS Earth Space Chem. 2021, 5, 1455−1467

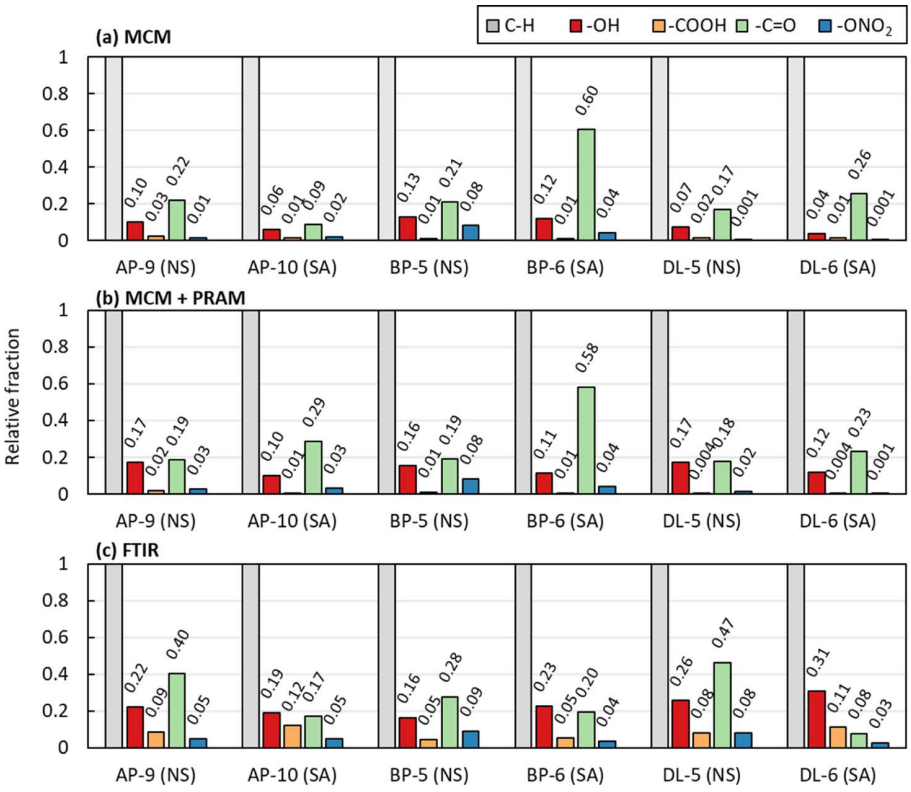

Figure 6. Relative functional composition of terpene SOA under two different seed conditions: NS and with SA estimated from (a) UNIPAR simulation with the gas kinetic mechanism of MCM v3.3.1; (b) UNIPAR simulation with the gas kinetic mechanism of the MCM v3.3.1 and PRAM; and (c) measured using a FTIR spectrometer. The *y*-axis shows the mole-based relative fraction of functional groups to C−H stretching. "AP", "BP", and "DL" denote α-pinene, β-pinene, and D-limonene, respectively. "NS" and "SA" represent the experiments in the absence of the seed and in the presence of the SA seed. The detailed experimental conditions are shown in Table S1.

in a less polluted environment where the hydrocarbon concentration is lower.

4.3. Model Uncertainties. For the formation of SOA, Figure 5 demonstrates the significance of the major model parameters such as the presence of PRAMs (Figure 5a), P_L (Figure 5b), γ_{in} (Figure 5c), and the rate constants (k_o and k_{AC}) for heterogeneous reactions (Figure 5d). With the addition of the PRAM to the MCM, OM_T of α-pinene and D-limonene SOA increases by 15−35% and by 71−119%, respectively, while that of β-pinene SOA slightly decreases (11−27% at high NO_x levels) or shows no change at the low NO_x levels. The PRAM improves the prediction of SOA formation by implementation of gas-phase autoxidation mechanisms. According to the reaction rate constant in the PRAM, the intramolecular H shift and autoxidation in the presence of O_2 are very fast with an estimated characteristic time of $\sim 10^1$ s, which is much shorter than the conventional reaction of alkene with OH radicals ($10^4 - 10^6$ s). For example, the reaction rate constant of α-pinene with the OH radical in the MCM is $\sim 5 \times 10^{-11}$ cm^3 molecule^{-1} s^{-1}. Assuming that the ambient OH radical concentration is $\sim 1 \times 10^6$ molecule cm^{-3},[78] the estimated characteristic time for α-pinene with the OH radical is $\sim 2 \times 10^4$ s. The PRAM utilizes the unified HOM precursor for all terpenes. However, the HOM precursor of D-limonene can produce different products from α-pinene because the remaining double bond in the D-limonene HOM precursor can react with atmospheric oxidants and yield organic compounds at different volatility and reactivity.

Both P_L and γ_{in} are important model parameters that influence the multiphase partitioning of organic species and further affect both OM_P and OM_{AR}. The reported uncertainty in P_L is 45% based on the group contribution method. By increasing/decreasing P_L for a factor of 1.5/0.5, the variation of the predicted OM_T is −19 to 74% (Figure 5b) compared to the reference condition. As described previously, γ_{in} (eq 3) is semiempirically estimated using a polynomial equation by fitting the predicted γ_{in} to the γ estimated using the AIOMFAC thermodynamic model.[62,79] AIOMFAC is a useful tool for predicting γ of inorganic and organic mixtures, but it has substantial uncertainty resulting from the limitation of the database. By increasing/decreasing γ_{in} for a factor of 2.0/0.5, the variation of the predicted OM_T is from — −26 to 70% (Figure 5c). The highest enhancement in SOA mass appears with D-limonene, especially in the presence of acidic seeds under high NO_x levels. Figure 5d illustrates the model uncertainties associated with the aerosol phase reaction rate constant (k_o and k_{AC}). The estimated uncertainties are relatively small, ranging from −15 to 14% for all three terpene SOAs when both k_o and k_{AC} change by a factor of 1.5 or 0.5.

The chamber simulations were generally performed with much higher hydrocarbon concentrations than those in ambient air due to the instrumental detection limits in both gaseous compounds and aerosol concentrations. The UNIAPR model reasonably simulates the chamber data that were obtained under various environmental conditions (types of hydrocarbons; different NO_x levels; dynamic meteorological conditions associated with temperature, humidity, and sun-

https://doi.org/10.1021/acsearthspacechem.1c00056
ACS Earth Space Chem. 2021, 5, 1455−1467

light; and the types of inorganic seed associated with hygroscopicity and aerosol acidity). Therefore, the UNIAPR model improves our understanding of SOA formation that occurs in ambient air.

4.4. Predicted SOA Composition Versus the FTIR Data. The model-predicted functional groups of three terpene SOA products were compared with the measurements obtained from FTIR spectra (Figure 6). The functionality composition normalized with the intensity of the C−H stretching band comprises C−H, −OH, −COOH, C═O, and $-ONO_2$. The observed carbonyl group (−C═O) in the presence of SA is significantly lower than that in the absence of the seed due to heterogeneous reactions of aldehydes.[21] In FTIR data for all three terpenes, the −C═O fraction in SA-seeded SOA is significantly less than that in non-seeded SOA, clearly showing the oligomerization of aldehyde products in the presence of SA seeds. The predicted −C═O in SA-seeded SOA is apparently greater than that in the non-seeded SOA because the model represents both the carbonyls, partitioned to aerosol, and the oligomeric products originating from the heterogeneous reactions of multi-functional aldehydes. The multi-functional aldehydes dissolved in the SA-seeded aqueous phase are rapidly transformed to the oligomeric products, which continuously promotes partitioning of aldehydes from the gas phase to the aerosol phase. The model-predicted functionality compositions with the MCM + PRAM were also compared with that with the MCM solely (Figure 6a,b). For all three precursors, the −OH group fractions increase by introducing the PRAM: 0.04−0.13 with the MCM and 0.10−0.17 with MCM + PRAM. Even with the PRAM, the simulated −OH fractions (Figure 6b) are still lower than those in the FTIR observations (Figure 6c). The simulated fractions of the $-ONO_2$ group were somewhat underestimated compared to the observations (0.02−0.09). In the presence of SA, the fraction of $-ONO_2$ decreased, indicating that some organic nitrates are unstable and hydrolyzed.

More importantly, the model significantly underestimates carboxylic acid (−COOH group) (Figure 6c). The formation of carboxylic acids from the oxidation of monoterpenes has been reported in numerous laboratory and field studies.[61,73,80−83] In general, the higher yields of carboxylic acids appear with ozonolysis of monoterpenes[61,84] and decrease with increasing the involvement of the reaction with OH radicals.[73] Despite numerous studies, the mechanisms to form carboxylic acids from the atmospheric processes of monoterpenes are still not well understood. Both gas-phase and aqueous-phase reaction pathways are possibly involved in forming carboxylic acids. For example, the recent laboratory study by Aljawhary et al.[85] proposed that 3-methyl-1,2,3-butanetricarboxylic acid, a major carboxylic acid from α-pinene, was formed via both the gas-phase oxidation pathway and the aqueous reaction pathway. Hence, further investigation for the formation of carboxylic acid products is needed. The carboxylic acid group typically reduces the vapor pressure of products. The discovery of the formation mechanisms of carboxylic acids possibly improves the prediction of aerosol compositions by increased contribution of the multi-functional products that contain both carboxylic acid and other polar functionalities (i.e., −C═O, −OH, and $-ONO_2$).

5. ATMOSPHERIC IMPLICATIONS

The UNIPAR model was demonstrated to predict the SOA mass produced via the photo-oxidation of terpene under varying NO_x and seed conditions. In the model, SOA formation was processed via multiphase partitioning (gas phase, organic phase, and inorganic phase) and in-particle chemistry of lumping species, which were explicitly predicted from the oxidation of terpene in the gas phase. Owing to the governmental efforts, 88% of total SO_2 emissions and 63% of total NO_x emissions have been reduced in North America between 1990 and 2018 (www.epa.gov/air-emissions-inventories/air-pollutant-emissions-trends-data). With these trends, acidic sulfate in aerosols has been gradually reduced. Despite the numerous efforts toward mitigation of SO_2 emissions, little response of aerosol pH was found throughout the continental US over the last 20 years due to gas−particle partitioning of ammonia and nitric acid.[86]

Importantly, the reduction of SO_2 can potentially decrease SOA mass, while the reduction of NO_x promotes SOA mass in urban and suburban areas. The simulation using the UNIPAR model provides insight into the impact of aerosol acidity and NO_x on SOA formation. AHS is atmospherically relevant and able to reasonably predict the terpene SOA under the acidic condition (Figure 4). In the presence of AHS, terpene SOA formation was considerably promoted by aerosol-phase reactions. Therefore, if the model does not include acid-driven in-particle chemistry, the terpene SOA mass can be significantly underestimated.

Additionally, the importance of in-particle chemistry on SOA mass varies with the NO_x level. In order to characterize the impact of the NO_x level, α-pinene SOA was simulated under various HC/NO_x ratios ranging from 3 to 50 ppbC/ppb as seen in Figure S11. The impact of aerosol acidity was greater at the high NO_x level. For example, the predicted α-pinene SOA mass with AHS (Figure S11c) is two times higher than the non-seeded SOA mass (Figure S11a) at $HC/NO_x = 3$. The gap in α-pinene SOA mass between AHS and non-seeded gradually decreases until HC/NO_x reaches to 10 (1.7 times). With changing HC/NO_x ratios from 3 to 16, SOA mass without seeds increases by 2.5 times (Figure S11a). For $HC/NO_x > 16$, α-pinene SOA mass is relatively insensitive to NO_x levels. The HC/NO_x ratio in Los Angeles is projected to change from 3 to 6 between the year 2000 to 2035.[87] Under this circumstance, α-pinene SOA mass will increase by 1.3 times based on UNIPAR simulation. The reduction of sulfate in the current trend can positively be attributed to the decrease in SOA mass, but the reduced NO_x enables an increase in SOA mass in urban areas where the NO_x level is high.

The NO_x regime can also influence terpene SOA formation. In general, the reaction of RO_2 with HO_2 radicals leads to relatively lower volatility products than the RO_2 with NO reaction.[75,88,89] In addition, HOM, a product from autoxidation, more efficiently forms at the lower NO_x level.[37] The contribution of HOM to SOA mass can be increased with decreasing NO_x, particularly in urban environments. For example, when the HC/NO_x ratio increases from 3 to 15 in the absence of acidic seeds (Figures S11a and S11b), the SOA mass related to HOM increases from 20 to 30%. However, Pye et al.[36] recently suggested that the autoxidation mechanism in terpene oxidation can be less critical to the total SOA in the chemical regime of the atmosphere changes compared to the one in which RO_2 autoxidation becomes extremely important (very low NO_x). The NO_x regime of this study was more relevant to changes in urban and suburban environments.

Currently, the regional air quality models [i.e., Community Multiscale Air Quality model (CMAQ, v5.1)] tend to

https://doi.org/10.1021/acsearthspacechem.1c00056
ACS Earth Space Chem. 2021, 5, 1455−1467

underestimate biogenic SOA.[16,90] Such underestimations can be partially caused by omitting aqueous reactions[91] of various oxidized products and by missing the gas-phase mechanisms to form less volatile products (i.e., HOM and carboxylic acids). Hitherto, the heterogeneous reactions of isoprene products have been implemented in the regional models,[1,92−94] but aqueous reactions of other products originating from various HCs (i.e., aromatic HCs, terpene HCs, alkanes, and various VOCs from consumer products) are still inaccessible.[5,6,8,95] The model parameters of this study were adjusted to chamber simulation that was influenced by the gas-wall partitioning of organic products.[96−98] In order to apply the UNIPAR model to the regional scale, the model parameters need to be revised by excluding the impact of the chamber wall on SOA formation.

■ ASSOCIATED CONTENT

Supporting Information

The Supporting Information is available free of charge at https://pubs.acs.org/doi/10.1021/acsearthspacechem.1c00056.

Experimental conditions and time profile; time profiles; group distribution of α-pinene lumping products; group distribution of β-pinene lumping products; group distribution of d-limonene lumping products; major lumping species of PRAM mechanism; estimation of diOS formation; simulated SOA formation associated with heterogeneous reactions and partitioning process; and sensitivity of UNIPAR-predicted terpene SOA mass (PDF)

■ AUTHOR INFORMATION

Corresponding Author

Myoseon Jang − *Department of Environmental Engineering Sciences, University of Florida, Gainesville 32611-6450, Florida, United States;* orcid.org/0000-0003-4211-7883; Phone: +1-352-846-1744; Email: mjang@ufl.edu

Authors

Zechen Yu − *Department of Environmental Engineering Sciences, University of Florida, Gainesville 32611-6450, Florida, United States;* orcid.org/0000-0002-6763-0520

Tianyu Zhang − *Department of Environmental Engineering Sciences, University of Florida, Gainesville 32611-6450, Florida, United States*

Azad Madhu − *Department of Environmental Engineering Sciences, University of Florida, Gainesville 32611-6450, Florida, United States*

Sanghee Han − *Department of Environmental Engineering Sciences, University of Florida, Gainesville 32611-6450, Florida, United States*

Complete contact information is available at: https://pubs.acs.org/10.1021/acsearthspacechem.1c00056

Notes

The authors declare no competing financial interest.

■ ACKNOWLEDGMENTS

This research was supported by the National Science Foundation (NSF#1923651) and the National Strategic Project-Fine particle of the National Research Foundation of Korea (NRF) funded by the Ministry of Science and ICT (MIST), the Ministry of Environment (ME), and the Ministry of Health and Welfare (MOHW) (2017M3D8A1090654).

■ REFERENCES

(1) Hallquist, M.; Wenger, J. C.; Baltensperger, U.; Rudich, Y.; Simpson, D.; Claeys, M.; Dommen, J.; Donahue, N. M.; George, C.; Goldstein, A. H.; Hamilton, J. F.; Herrmann, H.; Hoffmann, T.; Iinuma, Y.; Jang, M.; Jenkin, M. E.; Jimenez, J. L.; Kiendler-Scharr, A.; Maenhaut, W.; McFiggans, G.; Mentel, T. F.; Monod, A.; Prévôt, A. S. H.; Seinfeld, J. H.; Surratt, J. D.; Szmigielski, R.; Wildt, J. The Formation, Properties and Impact of Secondary Organic Aerosol: Current and Emerging Issues. *Atmos. Chem. Phys.* **2009**, *9*, 5155−5236.

(2) Jimenez, J. L.; Canagaratna, M. R.; Donahue, N. M.; Prevot, A. S. H.; Zhang, Q.; Kroll, J. H.; DeCarlo, P. F.; Allan, J. D.; Coe, H.; Ng, N. L.; Aiken, A. C.; Docherty, K. S.; Ulbrich, I. M.; Grieshop, A. P.; Robinson, A. L.; Duplissy, J.; Smith, J. D.; Wilson, K. R.; Lanz, V. A.; Hueglin, C.; Sun, Y. L.; Tian, J.; Laaksonen, A.; Raatikainen, T.; Rautiainen, J.; Vaattovaara, P.; Ehn, M.; Kulmala, M.; Tomlinson, J. M.; Collins, D. R.; Cubison, M. J.; Dunlea, J.; Huffman, J. A.; Onasch, T. B.; Alfarra, M. R.; Williams, P. I.; Bower, K.; Kondo, Y.; Schneider, J.; Drewnick, F.; Borrmann, S.; Weimer, S.; Demerjian, K.; Salcedo, D.; Cottrell, L.; Griffin, R.; Takami, A.; Miyoshi, T.; Hatakeyama, S.; Shimono, A.; Sun, J. Y.; Zhang, Y. M.; Dzepina, K.; Kimmel, J. R.; Sueper, D.; Jayne, J. T.; Herndon, S. C.; Trimborn, A. M.; Williams, L. R.; Wood, E. C.; Middlebrook, A. M.; Kolb, C. E.; Baltensperger, U.; Worsnop, D. R. Evolution of Organic Aerosols in the Atmosphere. *Science* **2009**, *326*, 1525−1529.

(3) Pope, C. A.; Ezzati, M.; Dockery, D. W. Fine-Particulate Air Pollution and Life Expectancy in the United States. *N. Engl. J. Med.* **2009**, *360*, 376−386.

(4) Kelly, J. M.; Doherty, R. M.; O'Connor, F. M.; Mann, G. W. The impact of biogenic, anthropogenic, and biomass burning volatile organic compound emissions on regional and seasonal variations in secondary organic aerosol. *Atmos. Chem. Phys.* **2018**, *18*, 7393−7422.

(5) Zhang, H.; Yee, L. D.; Lee, B. H.; Curtis, M. P.; Worton, D. R.; Isaacman-VanWertz, G.; Offenberg, J. H.; Lewandowski, M.; Kleindienst, T. E.; Beaver, M. R.; Holder, A. L.; Lonneman, W. A.; Docherty, K. S.; Jaoui, M.; Pye, H. O. T.; Hu, W.; Day, D. A.; Campuzano-Jost, P.; Jimenez, J. L.; Guo, H.; Weber, R. J.; de Gouw, J.; Koss, A. R.; Edgerton, E. S.; Brune, W.; Mohr, C.; Lopez-Hilfiker, F. D.; Lutz, A.; Kreisberg, N. M.; Spielman, S. R.; Hering, S. V.; Wilson, K. R.; Thornton, J. A.; Goldstein, A. H. Monoterpenes are the largest source of summertime organic aerosol in the southeastern United States. *Proc. Natl. Acad. Sci. U.S.A.* **2018**, *115*, 2038−2043.

(6) Pöschl, U.; Shiraiwa, M. Multiphase Chemistry at the Atmosphere-Biosphere Interface Influencing Climate and Public Health in the Anthropocene. *Chem. Rev.* **2015**, *115*, 4440−4475.

(7) Atkinson, R. Atmospheric chemistry of VOCs and NOx. *Atmos. Environ.* **2000**, *34*, 2063−2101.

(8) Jang, M.; Czoschke, N. M.; Lee, S.; Kamens, R. M. Heterogeneous atmospheric aerosol production by acid-catalyzed particle-phase reactions. *Science* **2002**, *298*, 814−817.

(9) Jang, M.; Czoschke, N. M.; Northcross, A. L.; Cao, G.; Shaof, D. SOA Formation from Partitioning and Heterogeneous Reactions: Model Study in the Presence of Inorganic Species. *Environ. Sci. Technol.* **2006**, *40*, 3013−3022.

(10) Tolocka, M. P.; Jang, M.; Ginter, J. M.; Cox, F. J.; Kamens, R. M.; Johnston, M. V. Formation of oligomers in secondary organic aerosol. *Environ. Sci. Technol.* **2004**, *38*, 1428−1434.

(11) Klodt, A. L.; Romonosky, D. E.; Lin, P.; Laskin, J.; Laskin, A.; Nizkorodov, S. A. Aqueous Photochemistry of Secondary Organic Aerosol of α-Pinene and α-Humulene in the Presence of Hydrogen Peroxide or Inorganic Salts. *ACS Earth Space Chem.* **2019**, *3*, 2736−2746.

(12) Lee, A.; Goldstein, A. H.; Kroll, J. H.; Ng, N. L.; Varutbangkul, V.; Flagan, R. C.; Seinfeld, J. H. Gas-phase products and secondary aerosol yields from the photooxidation of 16 different terpenes. *J. Geophys. Res.: Atmos.* **2006**, *111*, D17305.

(13) Friedman, B.; Farmer, D. K. SOA and gas phase organic acid yields from the sequential photooxidation of seven monoterpenes. *Atmos. Environ.* **2018**, *187*, 335−345.
(14) Zhao, D. F.; Kaminski, M.; Schlag, P.; Fuchs, H.; Acir, I.-H.; Bohn, B.; Häseler, R.; Kiendler-Scharr, A.; Rohrer, F.; Tillmann, R.; Wang, M. J.; Wegener, R.; Wildt, J.; Wahner, A.; Mentel, T. F. Secondary organic aerosol formation from hydroxyl radical oxidation and ozonolysis of monoterpenes. *Atmos. Chem. Phys.* **2015**, *15*, 991−1012.
(15) Claeys, M.; Graham, B.; Vas, G.; Wang, W.; Vermeylen, R.; Pashynska, V.; Cafmeyer, J.; Guyon, P.; Andreae, M. O.; Artaxo, P.; Maenhaut, W. Formation of secondary organic aerosols through photooxidation of isoprene. *Science* **2004**, *303*, 1173−1176.
(16) Ehn, M.; Thornton, J. A.; Kleist, E.; Sipilä, M.; Junninen, H.; Pullinen, I.; Springer, M.; Rubach, F.; Tillmann, R.; Lee, B.; Lopez-Hilfiker, F.; Andres, S.; Acir, I.-H.; Rissanen, M.; Jokinen, T.; Schobesberger, S.; Kangasluoma, J.; Kontkanen, J.; Nieminen, T.; Kurtén, T.; Nielsen, L. B.; Jørgensen, S.; Kjaergaard, H. G.; Canagaratna, M.; Maso, M. D.; Berndt, T.; Petäjä, T.; Wahner, A.; Kerminen, V.-M.; Kulmala, M.; Worsnop, D. R.; Wildt, J.; Mentel, T. F. A large source of low-volatility secondary organic aerosol. *Nature* **2014**, *506*, 476−479.
(17) Pankow, J. F. An absorption model of the gas/aerosol partitioning involved in the formation of secondary organic aerosol. *Atmos. Environ.* **1994**, *28*, 189−193.
(18) Odum, J. R.; Hoffmann, T.; Bowman, F.; Collins, D.; Flagan, R. C.; Seinfeld, J. H. Gas/particle partitioning and secondary organic aerosol yields. *Environ. Sci. Technol.* **1996**, *30*, 2580−2585.
(19) Donahue, N. M.; Robinson, A. L.; Stanier, C. O.; Pandis, S. N. Coupled partitioning, dilution, and chemical aging of semivolatile organics. *Environ. Sci. Technol.* **2006**, *40*, 2635−2643.
(20) Laskin, J.; Laskin, A.; Nizkorodov, S. A. Mass Spectrometry Analysis in Atmospheric Chemistry. *Anal. Chem.* **2018**, *90*, 166−189.
(21) Li, J.; Jang, M.; Beardsley, R. L. Dialkylsulfate formation in sulfuric acid-seeded secondary organic aerosol produced using an outdoor chamber under natural sunlight. *Environ. Chem.* **2016**, *13*, 590−601.
(22) Zhang, R.; Wang, G.; Guo, S.; Zamora, M. L.; Ying, Q.; Lin, Y.; Wang, W.; Hu, M.; Wang, Y. Formation of Urban Fine Particulate Matter. *Chem. Rev.* **2015**, *115*, 3803−3855.
(23) McNeill, V. F.; Woo, J. L.; Kim, D. D.; Schwier, A. N.; Wannell, N. J.; Sumner, A. J.; Barakat, J. M. Aqueous-Phase Secondary Organic Aerosol and Organosulfate Formation in Atmospheric Aerosols: A Modeling Study. *Environ. Sci. Technol.* **2012**, *46*, 8075−8081.
(24) Dawson, M. L.; Xu, J.; Griffin, R. J.; Dabdub, D. Development of aroCACM/MPMPO 1.0: A model to simulate secondary organic aerosol from aromatic precursors in regional models. *Geosci. Model Dev.* **2016**, *9*, 2143−2151.
(25) Couvidat, F.; Sartelet, K. The Secondary Organic Aerosol Processor (SOAP v1.0) model: a unified model with different ranges of complexity based on the molecular surrogate approach. *Geosci. Model Dev.* **2015**, *8*, 1111−1138.
(26) Beardsley, R. L.; Jang, M. Simulating the SOA Formation of Isoprene from Partitioning and Aerosol Phase Reactions in the Presence of Inorganics. *Atmos. Chem. Phys.* **2016**, *16*, 5993−6009.
(27) Im, Y.; Jang, M.; Beardsley, R. Simulation of aromatic SOA formation using the lumping model integrated with explicit gas-phase kinetic mechanisms and aerosol-phase reactions. *Atmos. Chem. Phys.* **2014**, *14*, 4013.
(28) Zhou, C.; Jang, M.; Yu, Z. Simulation of SOA formation from the photooxidation of monoalkylbenzenes in the presence of aqueous aerosols containing electrolytes under various NOx levels. *Atmos. Chem. Phys.* **2019**, *19*, 5719−5735.
(29) Crounse, J. D.; Nielsen, L. B.; Jørgensen, S.; Kjaergaard, H. G.; Wennberg, P. O. Autoxidation of Organic Compounds in the Atmosphere. *J. Phys. Chem. Lett.* **2013**, *4*, 3513−3520.
(30) Tröstl, J.; Chuang, W. K.; Gordon, H.; Heinritzi, M.; Yan, C.; Molteni, U.; Ahlm, L.; Frege, C.; Bianchi, F.; Wagner, R.; Simon, M.; Lehtipalo, K.; Williamson, C.; Craven, J. S.; Duplissy, J.; Adamov, A.; Almeida, J.; Bernhammer, A.-K.; Breitenlechner, M.; Brilke, S.; Dias, A.; Ehrhart, S.; Flagan, R. C.; Franchin, A.; Fuchs, C.; Guida, R.; Gysel, M.; Hansel, A.; Hoyle, C. R.; Jokinen, T.; Junninen, H.; Kangasluoma, J.; Keskinen, H.; Kim, J.; Krapf, M.; Kürten, A.; Laaksonen, A.; Lawler, M.; Leiminger, M.; Mathot, S.; Möhler, O.; Nieminen, T.; Onnela, A.; Petäjä, T.; Piel, F. M.; Miettinen, P.; Rissanen, M. P.; Rondo, L.; Sarnela, N.; Schobesberger, S.; Sengupta, K.; Sipilä, M.; Smith, J. N.; Steiner, G.; Tomè, A.; Virtanen, A.; Wagner, A. C.; Weingartner, E.; Wimmer, D.; Winkler, P. M.; Ye, P.; Carslaw, K. S.; Curtius, J.; Dommen, J.; Kirkby, J.; Kulmala, M.; Riipinen, I.; Worsnop, D. R.; Donahue, N. M.; Baltensperger, U. The role of low-volatility organic compounds in initial particle growth in the atmosphere. *Nature* **2016**, *533*, 527−531.
(31) Møller, K. H.; Praske, E.; Xu, L.; Crounse, J. D.; Wennberg, P. O.; Kjaergaard, H. G. Stereoselectivity in Atmospheric Autoxidation. *J. Phys. Chem. Lett.* **2019**, *10*, 6260−6266.
(32) Nah, T.; Sanchez, J.; Boyd, C. M.; Ng, N. L. Photochemical Aging of α-pinene and β-pinene Secondary Organic Aerosol formed from Nitrate Radical Oxidation. *Environ. Sci. Technol.* **2016**, *50*, 222−231.
(33) Bianchi, F.; Kurtén, T.; Riva, M.; Mohr, C.; Rissanen, M. P.; Roldin, P.; Berndt, T.; Crounse, J. D.; Wennberg, P. O.; Mentel, T. F.; Wildt, J.; Junninen, H.; Jokinen, T.; Kulmala, M.; Worsnop, D. R.; Thornton, J. A.; Donahue, N.; Kjaergaard, H. G.; Ehn, M. Highly Oxygenated Organic Molecules (HOM) from Gas-Phase Autoxidation Involving Peroxy Radicals: A Key Contributor to Atmospheric Aerosol. *Chem. Rev.* **2019**, *119*, 3472−3509.
(34) Kurtén, T.; Tiusanen, K.; Roldin, P.; Rissanen, M.; Luy, J.-N.; Boy, M.; Ehn, M.; Donahue, N. α-Pinene Autoxidation Products May Not Have Extremely Low Saturation Vapor Pressures Despite High O:C Ratios. *J. Phys. Chem. A* **2016**, *120*, 2569−2582.
(35) Draper, D. C.; Myllys, N.; Hyttinen, N.; Møller, K. H.; Kjaergaard, H. G.; Fry, J. L.; Smith, J. N.; Kurtén, T. Formation of Highly Oxidized Molecules from NO3 Radical Initiated Oxidation of Δ-3-Carene: A Mechanistic Study. *ACS Earth Space Chem.* **2019**, *3*, 1460−1470.
(36) Pye, H. O. T.; D'Ambro, E. L.; Lee, B. H.; Schobesberger, S.; Takeuchi, M.; Zhao, Y.; Lopez-Hilfiker, F.; Liu, J.; Shilling, J. E.; Xing, J.; Mathur, R.; Middlebrook, A. M.; Liao, J.; Welti, A.; Graus, M.; Warneke, C.; de Gouw, J. A.; Holloway, J. S.; Ryerson, T. B.; Pollack, I. B.; Thornton, J. A. Anthropogenic enhancements to production of highly oxygenated molecules from autoxidation. *Proc. Natl. Acad. Sci. U.S.A.* **2019**, *116*, 6641−6646.
(37) Roldin, P.; Ehn, M.; Kurtén, T.; Olenius, T.; Rissanen, M. P.; Sarnela, N.; Elm, J.; Rantala, P.; Hao, L.; Hyttinen, N.; Heikkinen, L.; Worsnop, D. R.; Pichelstorfer, L.; Xavier, C.; Clusius, P.; Öström, E.; Petäjä, T.; Kulmala, M.; Vehkamäki, H.; Virtanen, A.; Riipinen, I.; Boy, M. The role of highly oxygenated organic molecules in the Boreal aerosol-cloud-climate system. *Nat. Commun.* **2019**, *10*, 4370.
(38) Xavier, C.; Rusanen, A.; Zhou, P.; Dean, C.; Pichelstorfer, L.; Roldin, P.; Boy, M. Aerosol mass yields of selected biogenic volatile organic compounds - A theoretical study with nearly explicit gas-phase chemistry. *Atmos. Chem. Phys.* **2019**, *19*, 13741−13758.
(39) Jenkin, M. E.; Wyche, K. P.; Evans, C. J.; Carr, T.; Monks, P. S.; Alfarra, M. R.; Barley, M. H.; McFiggans, G. B.; Young, J. C.; Rickard, A. R. Development and chamber evaluation of the MCM v3.2 degradation scheme for β-caryophyllene. *Atmos. Chem. Phys.* **2012**, *12*, 5275−5308.
(40) Bertram, A. K.; Martin, S. T.; Hanna, S. J.; Smith, M. L.; Bodsworth, A.; Chen, Q.; Kuwata, M.; Liu, A.; You, Y.; Zorn, S. R. Predicting the relative humidities of liquid-liquid phase separation, efflorescence, and deliquescence of mixed particles of ammonium sulfate, organic material, and water using the organic-to-sulfate mass ratio of the particle and the oxygen-to-carbon elemental ratio of the organic component. *Atmos. Chem. Phys.* **2011**, *11*, 10995−11006.
(41) Chen, Q.; Heald, C. L.; Jimenez, J. L.; Canagaratna, M. R.; Zhang, Q.; He, L. Y.; Huang, X. F.; Campuzano-Jost, P.; Palm, B. B.; Poulain, L.; Kuwata, M.; Martin, S. T.; Abbatt, J. P. D.; Lee, A. K. Y.; Liggio, J. Elemental composition of organic aerosol: The gap between

https://doi.org/10.1021/acsearthspacechem.1c00056
ACS Earth Space Chem. 2021, 5, 1455−1467

ambient and laboratory measurements. *Geophys. Res. Lett.* **2015**, *42*, 4182−4189.
(42) You, Y.; Renbaum-Wolff, L.; Bertram, A. K. Liquid-liquid phase separation in particles containing organics mixed with ammonium sulfate, ammonium bisulfate, ammonium nitrate or sodium chloride. *Atmos. Chem. Phys.* **2013**, *13*, 11723−11734.
(43) You, Y.; Smith, M. L.; Song, M.; Martin, S. T.; Bertram, A. K. Liquid-liquid phase separation in atmospherically relevant particles consisting of organic species and inorganic salts. *Int. Rev. Phys. Chem.* **2014**, *33*, 43−77.
(44) Jiang, H.; Jang, M.; Yu, Z. Dithiothreitol activity by particulate oxidizers of SOA produced from photooxidation of hydrocarbons under varied NO x levels. *Atmos. Chem. Phys.* **2017**, *17*, 9965.
(45) Yu, Z.; Jang, M.; Sabo-Attwood, T.; Robinson, S. E.; Jiang, H. Prediction of Delivery of Organic Aerosols onto Air-liquid Interface Cells in Vitro Using an Electrostatic Precipitator. *Toxicol. in Vitro* **2017**, *42*, 319−328.
(46) Yu, Z.; Jang, M. Atmospheric Processes of Aromatic Hydrocarbons in the Presence of Mineral Dust Particles in an Urban Environment. *ACS Earth Space Chem.* **2019**, *3*, 2404−2414.
(47) Aiken, A. C.; Decarlo, P. F.; Kroll, J. H.; Worsnop, D. R.; Huffman, J. A.; Docherty, K. S.; Ulbrich, I. M.; Mohr, C.; Kimmel, J. R.; Sueper, D.; Sun, Y.; Zhang, Q.; Trimborn, A.; Northway, M.; Ziemann, P. J.; Canagaratna, M. R.; Onasch, T. B.; Alfarra, M. R.; Prevot, A. S. H.; Dommen, J.; Duplissy, J.; Metzger, A.; Baltensperger, U.; Jimenez, J. L. O/C and OM/OC Ratios of Primary, Secondary, and Ambient Organic Aerosols with High-resolution Time-of-flight Aerosol Mass Spectrometry. *Environ. Sci. Technol.* **2008**, *42*, 4478−4485.
(48) Canagaratna, M. R.; Jimenez, J. L.; Kroll, J. H.; Chen, Q.; Kessler, S. H.; Massoli, P.; Hildebrandt Ruiz, L.; Fortner, E.; Williams, L. R.; Wilson, K. R.; Surratt, J. D.; Donahue, N. M.; Jayne, J. T.; Worsnop, D. R. Elemental Ratio Measurements of Organic Compounds using Aerosol Mass Spectrometry: Characterization, Improved Calibration, and Implications. *Atmos. Chem. Phys.* **2015**, *15*, 253−272.
(49) Jang, M.; Kamens, R. M. Characterization of Secondary Aerosol from the Photooxidation of Toluene in the Presence of NOxand 1-Propene. *Environ. Sci. Technol.* **2001**, *35*, 3626−3639.
(50) Jang, M.; Sun, S.; Winslow, R.; Han, S.; Yu, Z. In situ aerosol acidity measurements using a UV-Visible micro-spectrometer and its application to the ambient air. *Aerosol. Sci. Technol.* **2020**, *54*, 446−461.
(51) Clegg, S. L.; Wexler, A. S. Densities and Apparent Molar Volumes of Atmospherically Important Electrolyte Solutions. 2. The Systems H^+− HSO_4^-− SO_4^{2-}− H_2O from 0 to 3 mol kg^{-1} as a Function of Temperature and H^+− NH_4^+− HSO_4^-− SO_4^{2-}− H_2O from 0 to 6 mol kg^{-1} at 25° C Using a Pitzer Ion Interaction Model, and NH_4HSO_4− H_2O and $(NH_4)_3H(SO_4)_2$− H_2O over the Entire Concentration Range. *J. Phys. Chem. A* **2011**, *115*, 3461−3474.
(52) Clegg, S. L.; Brimblecombe, P.; Wexler, A. S. Thermodynamic Model of the System H^+-NH_4^+-SO_4^{2-}-NO_3^--H_2O at Tropospheric Temperatures. *J. Phys. Chem. A* **1998**, *102*, 2137−2154.
(53) Li, J.; Jang, M. Aerosol acidity measurement using colorimetry coupled with a reflectance UV-visible spectrometer. *Aerosol. Sci. Technol.* **2012**, *46*, 833−842.
(54) Saunders, S. M.; Jenkin, M. E.; Derwent, R. G.; Pilling, M. J. Protocol for the development of the Master Chemical Mechanism, MCM v3 (Part A): tropospheric degradation of non-aromatic volatile organic compounds. *Atmos. Chem. Phys.* **2003**, *3*, 161−180.
(55) Jenkin, M. E.; Saunders, S. M.; Pilling, M. J. The tropospheric degradation of volatile organic compounds: a protocol for mechanism development. *Atmos. Environ.* **1997**, *31*, 81−104.
(56) Emmerson, K. M.; Evans, M. J. Comparison of Tropospheric Gas-phase Chemistry Schemes for Use within Global Models. *Atmos. Chem. Phys.* **2009**, *9*, 1831−1845.
(57) Roldin, P.; Ehn, M.; Kurtén, T.; Olenius, T.; Rissanen, M. P.; Sarnela, N.; Elm, J.; Rantala, P.; Hao, L.; Hyttinen, N.; Heikkinen, L.; Worsnop, D. R.; Pichelstorfer, L.; Xavier, C.; Clusius, P.; et al. The role of highly oxygenated organic molecules in the Boreal aerosol-cloud-climate system. *Nat. Commun.* **2019**, *10*, 4370 PANGAEA.Peroxy Radical Autoxidation Mechanism (PRAM)Supplement to:.
(58) Joback, K. G.; Reid, R. C. Estimation of pure-component properties from group-contributions. *Chem. Eng. Commun.* **1987**, *57*, 233−243.
(59) Stein, S. E.; Brown, R. L. Estimation of normal boiling points from group contributions. *J. Chem. Inf. Comput. Sci.* **1994**, *34*, 581−587.
(60) Zhao, L.; Li, P.; Yalkowsky, S. H. Predicting the entropy of boiling for organic compounds. *J. Chem. Inf. Comput. Sci.* **1999**, *39*, 1112−1116.
(61) Jang, M.; Kamens, R. M. Newly characterized products and composition of secondary aerosols from the reaction of α-pinene with ozone. *Atmos. Environ.* **1999**, *33*, 459−474.
(62) Zuend, A.; Marcolli, C.; Booth, A. M.; Lienhard, D. M.; Soonsin, V.; Krieger, U. K.; Topping, D. O.; McFiggans, G.; Peter, T.; Seinfeld, J. H. New and extended parameterization of the thermodynamic model AIOMFAC: calculation of activity coefficients for organic-inorganic mixtures containing carboxyl, hydroxyl, carbonyl, ether, ester, alkenyl, alkyl, and aromatic functional groups. *Atmos. Chem. Phys.* **2011**, *11*, 9155−9206.
(63) Schell, B.; Ackermann, I. J.; Hass, H.; Binkowski, F. S.; Ebel, A. Modeling the formation of secondary organic aerosol within a comprehensive air quality model system. *J. Geophys. Res. Atmos.* **2001**, *106*, 28275−28293.
(64) Cao, G.; Jang, M. An SOA model for toluene oxidation in the presence of inorganic aerosols. *Environ. Sci. Technol.* **2010**, *44*, 727−733.
(65) Press, W. H.; Teukolsky, S. A.; Vetterling, W. T.; Flannery, B. P. *Numerical Recipes in Fortran 77: The Art of Scientific Computing*; Cambridge university press Cambridge, 1992; Vol. 2.
(66) Odian, G. *Principles of Polymerization*; John Wiley & Sons, 2004.
(67) Faiola, C. L.; Buchholz, A.; Kari, E.; Yli-Pirilä, P.; Holopainen, J. K.; Kivimäenpää, M.; Miettinen, P.; Worsnop, D. R.; Lehtinen, K. E. J.; Guenther, A. B.; Virtanen, A. Terpene Composition Complexity Controls Secondary Organic Aerosol Yields from Scots Pine Volatile Emissions. *Sci. Rep.* **2018**, *8*, 3053.
(68) Malloy, Q. G. J.; Nakao, S.; Qi, L.; Austin, R.; Stothers, C.; Hagino, H.; Cocker, D. R., III Real-Time Aerosol Density Determination Utilizing a Modified Scanning Mobility Particle Sizer-Aerosol Particle Mass Analyzer System. *Aerosol. Sci. Technol.* **2009**, *43*, 673−678.
(69) Nakao, S.; Tang, P.; Tang, X.; Clark, C. H.; Qi, L.; Seo, E.; Asa-Awuku, A.; Cocker, D., III Density and elemental ratios of secondary organic aerosol: Application of a density prediction method. *Atmos. Environ.* **2013**, *68*, 273−277.
(70) Jang, M.; Czoschke, N. M.; Northcross, A. L. Semiempirical Model for Organic Aerosol Growth by Acid-Catalyzed Heterogeneous Reactions of Organic Carbonyls. *Environ. Sci. Technol.* **2005**, *39*, 164−174.
(71) Czoschke, N. M.; Jang, M. Acidity effects on the formation of α-pinene ozone SOA in the presence of inorganic seed. *Atmos. Environ.* **2006**, *40*, 4370−4380.
(72) Salo, K.; Hallquist, M.; Jonsson, Å. M.; Saathoff, H.; Naumann, K.-H.; Spindler, C.; Tillmann, R.; Fuchs, H.; Bohn, B.; Rubach, F.; Mentel, T. F.; Müller, L.; Reinnig, M.; Hoffmann, T.; Donahue, N. M. Volatility of secondary organic aerosol during OH radical induced ageing. *Atmos. Chem. Phys.* **2011**, *11*, 11055−11067.
(73) Hammes, J.; Lutz, A.; Mentel, T.; Faxon, C.; Hallquist, M. Carboxylic acids from limonene oxidation by ozone and hydroxyl radicals: insights into mechanisms derived using a FIGAERO-CIMS. *Atmos. Chem. Phys.* **2019**, *19*, 13037−13052.
(74) Jokinen, T.; Berndt, T.; Makkonen, R.; Kerminen, V.-M.; Junninen, H.; Paasonen, P.; Stratmann, F.; Herrmann, H.; Guenther, A. B.; Worsnop, D. R.; Kulmala, M.; Ehn, M.; Sipilä, M. Production of extremely low volatile organic compounds from biogenic emissions:

https://doi.org/10.1021/acsearthspacechem.1c00056
ACS Earth Space Chem. 2021, 5, 1455−1467

Measured yields and atmospheric implications. *Proc. Natl. Acad. Sci. U.S.A.* **2015**, *112*, 7123−7128.
(75) Ng, N. L.; Chhabra, P. S.; Chan, A. W. H.; Surratt, J. D.; Kroll, J. H.; Kwan, A. J.; McCabe, D. C.; Wennberg, P. O.; Sorooshian, A.; Murphy, S. M.; Dalleska, N. F.; Flagan, R. C.; Seinfeld, J. H. Effect of NOx level on secondary organic aerosol (SOA) formation from the photooxidation of terpenes. *Atmos. Chem. Phys.* **2007**, *7*, 5159−5174.
(76) Presto, A. A.; Huff Hartz, K. E.; Donahue, N. M. Secondary Organic Aerosol Production from Terpene Ozonolysis. 2. Effect of NOxConcentration. *Environ. Sci. Technol.* **2005**, *39*, 7046−7054.
(77) Santiago, M.; Vivanco, M. G.; Stein, A. F. SO2 effect on secondary organic aerosol from a mixture of anthropogenic VOCs: experimental and modelled results. *Int. J. Environ. Pollut.* **2012**, *50*, 224−233.
(78) Altshuller, A. P. Ambient air hydroxyl radical concentrations: Measurements and model predictions. *JAPCA* **1989**, *39*, 704−708.
(79) Zuend, A.; Marcolli, C.; Luo, B. P.; Peter, T. A thermodynamic model of mixed organic-inorganic aerosols to predict activity coefficients. *Atmos. Chem. Phys.* **2008**, *8*, 4559−4593.
(80) Chhabra, P. S.; Ng, N. L.; Canagaratna, M. R.; Corrigan, A. L.; Russell, L. M.; Worsnop, D. R.; Flagan, R. C.; Seinfeld, J. H. Elemental composition and oxidation of chamber organic aerosol. *Atmos. Chem. Phys.* **2011**, *11*, 8827−8845.
(81) Jenkin, M. E. Modelling the formation and composition of secondary organic aerosol from α- and β-pinene ozonolysis using MCM v3. *Atmos. Chem. Phys.* **2004**, *4*, 1741−1757.
(82) Kristensen, K.; Cui, T.; Zhang, H.; Gold, A.; Glasius, M.; Surratt, J. D. Dimers in α-pinene secondary organic aerosol: effect of hydroxyl radical, ozone, relative humidity and aerosol acidity. *Atmos. Chem. Phys.* **2014**, *14*, 4201−4218.
(83) Russell, L. M.; Bahadur, R.; Ziemann, P. J. Identifying organic aerosol sources by comparing functional group composition in chamber and atmospheric particles. *Proc. Natl. Acad. Sci. U.S.A.* **2011**, *108*, 3516−3521.
(84) Yu, J.; Cocker III, D. R.; Griffin, R. J.; Flagan, R. C.; Seinfeld, J. H. Gas-phase ozone oxidation of monoterpenes: Gaseous and particulate products. *J. Atmos. Chem.* **1999**, *34*, 207−258.
(85) Aljawhary, D.; Zhao, R.; Lee, A. K. Y.; Wang, C.; Abbatt, J. P. D. Kinetics, Mechanism, and Secondary Organic Aerosol Yield of Aqueous Phase Photo-oxidation of α-Pinene Oxidation Products. *J. Phys. Chem. A* **2016**, *120*, 1395−1407.
(86) Pye, H. O. T.; Nenes, A.; Alexander, B.; Ault, A. P.; Barth, M. C.; Clegg, S. L.; Collett Jr, J. L., Jr; Fahey, K. M.; Hennigan, C. J.; Herrmann, H.; Kanakidou, M.; Kelly, J. T.; Ku, I.-T.; McNeill, V. F.; Riemer, N.; Schaefer, T.; Shi, G.; Tilgner, A.; Walker, J. T.; Wang, T.; Weber, R.; Xing, J.; Zaveri, R. A.; Zuend, A. The acidity of atmospheric particles and clouds. *Atmos. Chem. Phys.* **2020**, *20*, 4809−4888.
(87) Zhao, Y.; Mao, P.; Zhou, Y.; Yang, Y.; Zhang, J.; Wang, S.; Dong, Y.; Xie, F.; Yu, Y.; Li, W. Improved provincial emission inventory and speciation profiles of anthropogenic non-methane volatile organic compounds: a case study for Jiangsu, China. *Atmos. Chem. Phys.* **2017**, *17*, 7733−7756.
(88) Zhao, D.; Schmitt, S. H.; Wang, M.; Acir, I.-H.; Tillmann, R.; Tan, Z.; Novelli, A.; Fuchs, H.; Pullinen, I.; Wegener, R.; Rohrer, F.; Wildt, J.; Kiendler-Scharr, A.; Wahner, A.; Mentel, T. F. Effects of NOx and SO2 on the secondary organic aerosol formation from photooxidation of α-pinene and limonene. *Atmos. Chem. Phys.* **2018**, *18*, 1611−1628.
(89) Pullinen, I.; Schmitt, S.; Kang, S.; Sarrafzadeh, M.; Schlag, P.; Andres, S.; Kleist, E.; Mentel, T. F.; Rohrer, F.; Springer, M.; Tillmann, R.; Wildt, J.; Wu, C.; Zhao, D.; Wahner, A.; Kiendler-Scharr, A. Impact of NOx on secondary organic aerosol (SOA) formation from α-pinene and β-pinene photooxidation: the role of highly oxygenated organic nitrates. *Atmos. Chem. Phys.* **2020**, *20*, 10125−10147.
(90) Pye, H. O. T.; Luecken, D. J.; Xu, L.; Boyd, C. M.; Ng, N. L.; Baker, K. R.; Ayres, B. R.; Bash, J. O.; Baumann, K.; Carter, W. P. L.; Edgerton, E.; Fry, J. L.; Hutzell, W. T.; Schwede, D. B.; Shepson, P. B. Modeling the Current and Future Roles of Particulate Organic Nitrates in the Southeastern United States. *Environ. Sci. Technol.* **2015**, *49*, 14195−14203.
(91) Pye, H. O. T.; Murphy, B. N.; Xu, L.; Ng, N. L.; Carlton, A. G.; Guo, H.; Weber, R.; Vasilakos, P.; Appel, K. W.; Budisulistiorini, S. H.; Surratt, J. D.; Nenes, A.; Hu, W.; Jimenez, J. L.; Isaacman-VanWertz, G.; Misztal, P. K.; Goldstein, A. H. On the implications of aerosol liquid water and phase separation for organic aerosol mass. *Atmos. Chem. Phys.* **2017**, *17*, 343−369.
(92) Ervens, B.; Turpin, B. J.; Weber, R. J. Secondary organic aerosol formation in cloud droplets and aqueous particles (aqSOA): a review of laboratory, field and model studies. *Atmos. Chem. Phys.* **2011**, *11*, 11069−11102.
(93) Pye, H. O. T.; Pinder, R. W.; Piletic, I. R.; Xie, Y.; Capps, S. L.; Lin, Y.-H.; Surratt, J. D.; Zhang, Z.; Gold, A.; Luecken, D. J.; Hutzell, W. T.; Jaoui, M.; Offenberg, J. H.; Kleindienst, T. E.; Lewandowski, M.; Edney, E. O. Epoxide Pathways Improve Model Predictions of Isoprene Markers and Reveal Key Role of Acidity in Aerosol Formation. *Environ. Sci. Technol.* **2013**, *47*, 11056−11064.
(94) Mao, J.; Carlton, A.; Cohen, R. C.; Brune, W. H.; Brown, S. S.; Wolfe, G. M.; Jimenez, J. L.; Pye, H. O. T.; Lee Ng, N.; Xu, L.; McNeill, V. F.; Tsigaridis, K.; McDonald, B. C.; Warneke, C.; Guenther, A.; Alvarado, M. J.; de Gouw, J.; Mickley, L. J.; Leibensperger, E. M.; Mathur, R.; Nolte, C. G.; Portmann, R. W.; Unger, N.; Tosca, M.; Horowitz, L. W. Southeast Atmosphere Studies: learning from model-observation syntheses. *Atmos. Chem. Phys.* **2018**, *18*, 2615−2651.
(95) Zhang, X.; Mcvay, R. C.; Huang, D. D.; Dalleska, N. F.; Aumont, B.; Flagan, R. C.; Seinfeld, J. H. Formation and evolution of molecular products in α-pinene secondary organic aerosol. *Proc. Natl. Acad. Sci. U.S.A.* **2015**, *112*, 14168−14173.
(96) Charan, S. M.; Huang, Y.; Seinfeld, J. H. Computational Simulation of Secondary Organic Aerosol Formation in Laboratory Chambers. *Chem. Rev.* **2019**, *119*, 11912−11944.
(97) McVay, R. C.; Cappa, C. D.; Seinfeld, J. H. Vapor-Wall Deposition in Chambers: Theoretical Considerations. *Environ. Sci. Technol.* **2014**, *48*, 10251−10258.
(98) Han, S.; Jang, M. Simulating the impact of gas-wall partitioning on SOA formation using the explicit gas mechanism integrated with aqueous reactions containing electrolytes. *Sci. Total Environ.* **2020**, *748*, 141360.

https://doi.org/10.1021/acsearthspacechem.1c00056
ACS Earth Space Chem. 2021, 5, 1455−1467